Substructure formation during pattern transposition from substrate into polymer blend film



2003 Europhys. Lett. 62 855

(http://iopscience.iop.org/0295-5075/62/6/855)

EUROPHYSICS LETTERS 15 June 2003

*Europhys. Lett.*, **62** (6), pp. 855–861 (2003)

# Substructure formation during pattern transposition from substrate into polymer blend film

P. Cyganik[1], A. Budkowski[1](*), U. Steiner[2], J. Rysz[1], A. Bernasik[3], S. Walheim[4], Z. Postawa[1] and J. Raczkowska[1]

[1] *M. Smoluchowski Institute of Physics, Jagellonian University Reymonta 4, 30-059 Kraków, Poland*

[2] *Department of Polymer Chemistry, University of Groningen 9747 AG Groningen, The Netherlands*

[3] *Faculty of Physics and Nuclear Techniques, University of Mining and Metallurgy Reymonta 23, 30-059 Kraków, Poland*

[4] *Institut für Nanotechnologie, Forschungszentrum Karlsruhe Postfach 3640, 76021 Karlsruhe, Germany*

(received 19 February 2003; accepted in final form 29 April 2003)

PACS. 61.41.+e – Polymers, elastomers, and plastics.
PACS. 64.75.+g – Solubility, segregation, and mixing; phase separation.
PACS. 68.55.-a – Thin film structure and morphology.

**Abstract.** – A chemical pattern on a substrate is transposed into thin films of a ternary polymer blend during spin-casting from a common solvent. One of the blend components intercalates at interfaces between the other two phases to reduce their interfacial energy. As a result, an extensive substructure is formed, in addition to domains with pattern periodicity $\lambda$. Morphologies with well-ordered lateral domains are created not only when the inherent scale of the phase domains $R$ is comparable to $\lambda$ (as observed previously) but also for $R \sim \lambda/2$, extending pattern transposition to smaller length scales.

Polymer films with a controlled morphology are technologically important in diverse fields, such as fabrication of electronic and optical devices or nano-lithographic templates. This has stimulated numerous studies on self-organization processes such as self-stratification [1] or pattern transposition [2–7]. In particular, the ordering of (micro-)phase domains in the presence of a homogeneous or pre-patterned (with periodicity $\lambda$) surface was studied. Domain morphology is controlled by many parameters, mainly by the competition between surface and interfacial energy [1, 7]. When a substrate is patterned, one of the problems is the commensuration between $\lambda$ and the inherent domain scale $R$ [2–7]. Only for $R$ matching $\lambda$, a pattern-echoing morphology with well-ordered domains is formed in diblock copolymer films cast onto a substrate with a chemical [2] or symmetric topographic [3] pattern. Investigations of polymer blend demixing during spin-casting (solvent quench) led to the identical conclusion for thin films on chemically patterned surfaces [2(a), 4, 5]. The time-dependent film

(*) E-mail: ufbudkow@cyf-kr.edu.pl

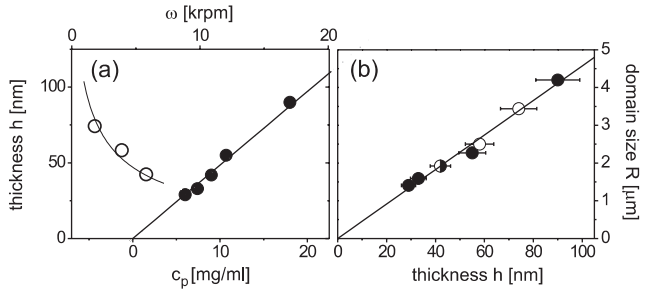


Fig. 1 – Characteristic length scales of dPS/PVP/PMMA (2:2:1) blend films on Au substrates stripe-patterned with a SAM. (a) Film thickness $h$ as a function of spin-casting speed $\omega$ (○, upper abscissa) and polymer concentration $c_{\mathrm{P}}$ (●, lower abscissa) for constant $c_{\mathrm{P}} = 9\,\mathrm{mg/ml}$ and $\omega = 5.8\,\mathrm{krpm}$, respectively. Solid lines, added for comparison, mark the relation $h \sim c_{\mathrm{P}}/\omega^{1/2}$. (b) Inherent scale of lateral domains $R$ plotted against $h$. The solid line indicates a linear fit.

morphology of polymer mixtures after a temperature quench [6] displayed highest order for $R(t) \sim \lambda$, but in addition exhibited for $R(t) \sim \lambda/n$ ($n = 2, 3, 4$) the excitation of weak free surface undulations coupled with the phase separation process. Transient substructures with half the substrate pattern periodicity were observed at flat surfaces of polymer blend films in recent simulations [7(a)].

In this letter, we present a detailed study on a model ternary polymer blend of deuterated polystyrene (dPS)/polyvinylpyridine (PVP)/poly(methyl methacrylate) (PMMA). Demixing due to a solvent quench on a patterned substrate led to the formation of thin-film morphologies, which were well ordered not only for $R \sim \lambda$, but also for $R \sim \lambda/2$. This is enabled by the formation of an extensive substructure as the PMMA blend component intercalates at the interfaces between the dPS and PVP phases to reduce their interfacial energy [8(a)]. The overall phase domain structure is mirrored by the surface topography. The film morphology was examined for different spin-casting conditions (that varied $R$) followed by a fast Fourier transform (FFT) analysis of topographic images. While most of the results presented here were for the optimal relative mass fraction of the interfacial-active blend component (PMMA), *i.e.* for the dPS/PVP/PMMA (2:2:1) mixture, the $R \sim \lambda/2$ situation is also illustrated for the 1:1:1 and 1:1:0 ratios.

Blend films of dPS ($M_{\mathrm{w}} = 174\,\mathrm{k}$, $M_{\mathrm{w}}/M_{\mathrm{n}} = 1.03$)/PVP ($M_{\mathrm{w}} = 115\,\mathrm{k}$, $M_{\mathrm{w}}/M_{\mathrm{n}} = 1.02$)/PMMA ($M_{\mathrm{w}} = 149\,\mathrm{k}$, $M_{\mathrm{w}}/M_{\mathrm{n}} = 1.10$) [8(a), 9] were spin-cast from tetrahydrofuran (TFH) solutions onto Au-covered Si wafers patterned with a self-assembled monolayer (SAM) of hexadecanethiol [$HS(CH_2)_{15}CH_3$]. The substrate pattern consisted of alternating (with $\lambda = 4.0(1)\,\mu$m [5] and ca. $2\,\mu$m wide) stripes of pure Au and SAM prepared using the micro-contact printing method [10]. The control samples were cast onto homogeneous SAM layers covering Au. Topographic (AFM) and lateral-force (LFM) images of thin films were acquired by a CP Park Scientific Instruments atomic-force microscope working in contact mode. LFM resolves domains rich in dPS, PVP and PMMA [9]. PVP composition maps with a lateral resolution of 120 nm were imaged for successive film depths by a mapping mode of a dynamic secondary ion mass spectrometry (dSIMS) [11] using $CN^-$ ions ($m/z = 26$). The overall phase domain structure, determined from the dSIMS and LFM data, was confirmed by AFM combined with selective dissolution of PVP and dPS [9]. The average film thickness $h$ (determined by AFM as described earlier [9]) was controlled by varying the spin-cast speed $\omega$ and polymer concentration $c_{\mathrm{P}}$ in THF (fig. 1(a)). Relations for $h(c_{\mathrm{P}})$ and $h(\omega)$ (observed

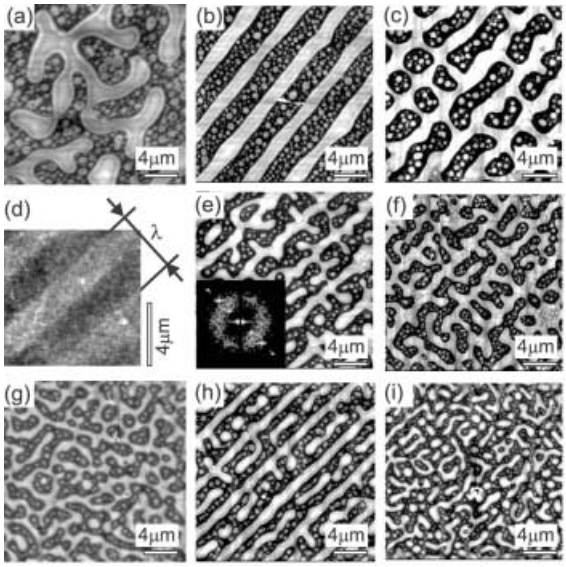


Fig. 2

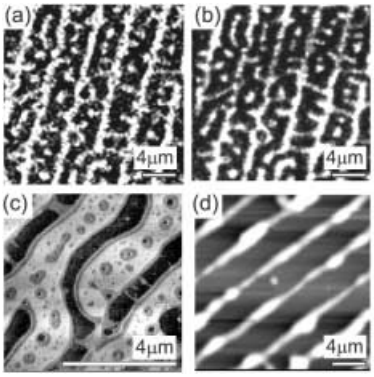


Fig. 3

Fig. 2 – AFM images of dPS/PVP/PMMA (2:2:1) blend films on homogeneous SAM substrates (a), (g), and on Au patterned with a SAM (b)-(c), (e)-(f) and (h)-(i). Film morphologies for $h = 90(10)$ (a)-(b), 74(5) (c), 58(6) (e), 55(5) (f), 42(4) (g)-(h), and 29(3) nm (i). The height range is roughly 55–65% of $h$. (d) LFM image of the substrate pattern (with periodicity $\lambda = 4\,\mu$m). To improve contrast, the original Au stripes were covered with $HS(CH_2)_{15}COOH$ [5] (light regions) prior to examination. The inset in (e) displays results of FFT analysis of the corresponding AFM image. Isotropic (diffuse ring) and anisotropic (diffraction peaks) components of FFT spectra are analyzed separately to determine $R$ (fig. 1(b)) and characterize pattern transposition (fig. 4).

Fig. 3 – Domain structure (a)-(c) and surface topography (d) of dPS/PVP/PMMA (2:2:1) blend films with $h = 58(6)$ (a)-(b) (cf. fig. 2(e)) and 42(4) nm (c)-(d) (cf. fig. 2(h)). Similar PVP (white) distribution maps recorded by dSISM [11] at distance $z \sim 15$ (a) and 44 nm (b) from the surface confirm the lateral character of film morphology [8(a), 9]. (c) The LFM image [9] confirms that PMMA (gray) separates domains rich in dPS (white) and PVP (black) [8(a), 9]. (d) AFM image of a film, which was additionally annealed for 60 min at 145 °C.

for a constant speed $\omega = 5.8$ k rpm and concentration $c_P = 9$ mg/ml) seem to follow the prediction $h \sim c_P/\omega^{1/2}$ [12(a)], as found previously for the same blend cast at constant $\omega$ on homogeneous SAM substrates [9].

We start with initial examination of the effect of a substrate pattern (presented in fig. 2(d)) on the free surface undulations observed by AFM for various spin-casting conditions of the dPS/PVP/PMMA (2:2:1) blend films. Figures 2(a) and (g) illustrate the topography of the film, cast onto homogeneous SAM substrates with thicknesses $h = 90(10)$ and $h = 42(4)$ nm, respectively. We notice morphologies with two dominant length scales, which decrease monotonically [9] as a function of $h$. Large-scale, elongated and almost continuous elevations coexist with much smaller circular protrusions [8(a), 9]. Figures 2(b)-(c), (e)-(f) and (h)-(i) show the topography of the same blend films, but cast onto Au patterned with a SAM, presented for successively decreasing film thicknesses $h = 90(10)$ to 29(3) nm. The first image of this series illustrates large-scale elevations forming a striped structure echoing (with periodicity $\lambda$) the

substrate pattern. Subsequent figures show that these elevations are linked by bridges, which evolve into well-ordered elongated domains of the $\lambda/2$-substructure. Finally, anisotropic morphologies are formed without a clear distinction between the primary $\lambda$-structure and the substructure. These features correspond to large-scale structures (characterized by $R$), which are always accompanied by secondary structures of much smaller circular protrusions.

The inset in fig. 2(e) represents the 2D FFT spectrum that corresponds to the AFM image in the main figure. It is typical for all the blend films cast on patterned substrates. The FFT image consists of an anisotropic component, characterized by a diagonal line of diffraction peaks with $\boldsymbol{k} = n\boldsymbol{k}_\lambda$ ($n$ is an integer) and a diffusive ring with $|\boldsymbol{k}| = k^*$. The two components were analyzed separately (see [5, 6, 9] for details). Squared FFT amplitudes of the $\boldsymbol{k}$-region forming a narrow (4 pixels wide) stripe along the peaks $n\boldsymbol{k}_\lambda$ were averaged to yield a power spectrum $P_{\mathrm{a}}(k)$ of the anisotropic FFT component, discussed in detail later. In the case of the radially isotropic FFT component, the radial averaged FFT data of the $\boldsymbol{k}$-plane (without $n\boldsymbol{k}_\lambda$-stripe) were used to measure the radius $k^*$ of the diffusive ring at its maximum to determine the inherent domain scale $R = 1/k^*$. Results of such a procedure are presented in fig. 1(b), where the plot of $R$ *vs.* the film thickness $h$ is shown. The two data sets, corresponding to films cast from solutions with differing polymer concentrations $c_{\mathrm{P}}$ (•) or rotation speeds $\omega$ (○) collapse, forming one master line. This indicates that $h$ reflects the spin-casting conditions in a well-defined manner. Identical $R$-values were found for the films with the same $h$, cast onto homogeneous SAM surfaces, as well as on patterned Au/SAM surfaces.

The phase separation that occurs during spin-casting is a complex process. Since solvent evaporation is fast, changes that occur within the film cannot be described using quasi-static models [13]. During film formation, various hydrodynamic regimes are thought to occur. In addition, the lack of sufficient equilibration often leads to long-lived metastable phase morphologies [8(b)]. In the absence of a suitable theoretical model of demixing during a solvent quench, we resort to a qualitative description [8, 9, 12] instead (an alternative can be found in [13]). Polymers dissolved in THF form initially a homogeneous liquid film. Liquid flow, that is caused by a balance between centrifugal and viscous forces, decreases film thickness and controls its final value $h$ [12(a)]. Phase separation, initiated by evaporating THF, takes place in a certain range of decreasing solvent concentration and terminates when the polymer molecules are no longer mobile. For thicker films, solvent drying and phase coarsening [14] take place during a longer period of time, leading to a monotonic relation between $h$ and the domain scale $R$ (fig. 1(b)). Coarsening domains are constrained by both film surfaces to form lateral morphologies [8]. While neither of the polymer blend phases wets the free surface or the SAM-covered substrate regions [8(a), 9], PVP exhibits a strong affinity to the Au stripes [4, 5], driving the organization of the lateral domains (fig. 3(a)-(b)). The lateral film morphology is governed by three interaction parameters: $\chi_{\mathrm{dPS/PVP}} = 0.1 \gg \chi_{\mathrm{dPS/PMMA}} \approx 0.02$, $\chi_{\mathrm{PVP/PMMA}} \approx 0.007$ [8(a)]. To reduce the interfacial energy, PMMA intercalates at the dPS/PVP interfaces [8(a), 9] and separates dPS- and PVP-rich phases (fig. 3(c)). PMMA enhances blend compatibility and increases the interfacial area, leading to extensive substructures (fig. 2) that are dominant in blends with nearly bicontinuous lateral morphologies. Such morphologies are accompanied by a secondary phase separation process [9, 12(b)-(d)], resulting in secondary structures of much smaller circular inclusions in the dPS-rich domains (fig. 3(c)). In the final solvent-free film, the phase morphology is mirrored by distinct topographic elevations, which stem from the differing solubility of the three polymers in THF [8]. PVP and PMMA solidify earlier than dPS, leading to a collapse of the initially THF-swollen PS domains below the level of PVP- and PMMA-rich domains [8, 9]. The lower surface regions correspond to dPS-rich domains, while elevated areas are PVP and PMMA (compare figs. 3(c) and 2(h)). This relation between topography and the overall domain

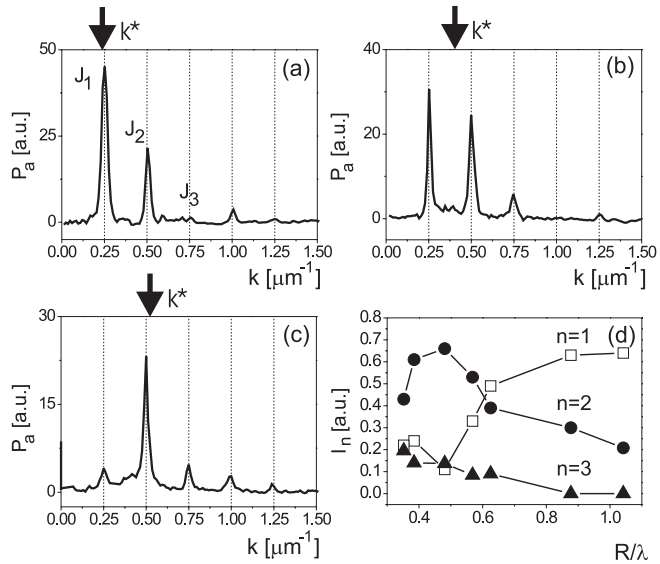


Fig. 4 – (a)-(c) Power spectra $P_a(k)$ [5, 6, 9] computed for the anisotropic FFT component of AFM images of dPS/PVP/PMMA (2:2:1) blend films with $h = 90(10)$ (a), 58(6) (b) and 42(4) nm (c). Positions of wave vector $k^* = 1/R$ are marked by arrows. $J_n$ ($n = 1, 2, 3$) denotes the intensity of peaks positioned at $nk_\lambda$ ($k_\lambda = 1/\lambda$). (d) Relative intensities $I_n = J_n/\Sigma_m J_m$ ($n = 1, 2, 3$) plotted *vs.* the degree of commensurability $R/\lambda$.

structure, valid for all spin-casting conditions [9], allows us to characterize film morphology using AFM data.

To study the compliance of the film morphology (characterized by the average domain size $R$) with the substrate pattern periodicity $\lambda$, we have analyzed the power spectra $P_a(k)$ reflecting the anisotropic FFT component of AFM images. $P_a(k)$ spectra (*e.g.*, figs. 4(a)-(c)) exhibit several sharp peaks positioned at $nk_\lambda$ ($k_\lambda = 1/\lambda$), characterized by absolute $J_n = J(nk_\lambda)$ and relative $I_n = J_n/\Sigma_m J_m$ intensities. Such an analysis, performed for the topographic data, is representative for the entire film morphology, the surface topography as well as the domain structure. For instance, almost identical $P_a(k)$ spectra were obtained for the AFM image with $I_1 = 0.49(2)$, $I_2 = 0.39(2)$, $I_3 = 0.09(2)$ (fig. 4(b)) and the dSIMS map of PVP distribution ($I_1 = 0.54(2)$, $I_2 = 0.42(2)$, $I_3 = 0.05(2)$) of the same film. Similar conclusions were reported for the dPS/PVP blend [5]. The peak intensities vary with the inherent domain size $R$ (wave vector $k^* = 1/R$) as shown in figs. 4(a)-(c) and summarized in fig. 4(d). The spectra are dominated by the peaks $k_\lambda$ and $2k_\lambda$, corresponding to the primary structure and the $\lambda/2$-substructure. In general, $I_1$ increases with $R$, but in addition to the maximal value observed at $R \sim \lambda$ it also exhibits a local minimum at $R \sim \lambda/2$. $I_2$ reaches its maximum at $R \sim \lambda/2$, which is slightly higher than the $I_1$ value at $R \sim \lambda$, and decreases for large $R$. Our results may be compared to the $\lambda/2$-substructures observed in recent computer simulations at flat free surfaces of blend films, which resulted from a competition between surface-directed and lateral phase separation [7(a)]. In our case, however, the surface-directed separation mode is negligible. In contrast to our results, a monotonic growth of the fundamental intensity $J_1$ and the excitation of weaker intensities $J_n$ ($n > 1$) at $R \sim \lambda/n$ was observed in [6], where free surface undulations were coupled with phase separation process. Here, the lateral large-scale phase domain structure is frozen-in, prior to

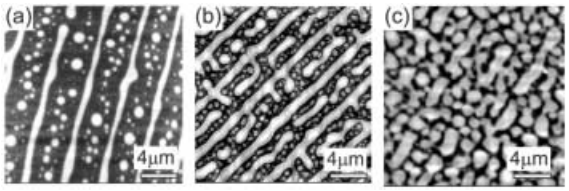


Fig. 5 – AFM images of dPS/PVP/PMMA blend films with relative polymer mass fractions 1:1:0 (a), 2:2:1 (b), and 1:1:1 (c) cast on Au patterned with a SAM for $R/\lambda = 0.52(4)$ (a), 0.48(4) (b), and 0.47(4) c). $\lambda/2$-substructure formation is most effective for the 2:2:1 blend (b) as indicated by relative intensities $I_2 = 0.43(2)$ (a), 0.67(2) (b), 0.57(3) and $I_1 = 0.20(2)$ (a), 0.11(2) (b), 0.23(3) (c).

the formation of topographic features reflecting the domain morphology [8, 12(c)-(d)].

The film morphology, formed at given spin-casting conditions, is far from thermal equilibrium [8] and corresponds to a certain (frozen) stage in the phase domain evolution. For instance, additional annealing of the film with the initial morphology shown in fig. 2(h) results in linear domains of the primary structure and no trace of the $\lambda/2$-substructure (fig. 3(d)). The sequence of frozen morphologies (figs. 2 from (i) to (a) except (d)) for increasing solvent drying time (*i.e.* film thickness $h$) corresponds to a growing inherent size $R$ of coarsening lateral domains [14]. The ordering of the phase domains is a consequence of the preferential adsorption of one blend phase to one of two stripe types, forming the substrate pattern, and the absence of such an adsorption to the second stripe type. This situation (not studied in computer simulations so far [7]) leads not only to the formation of the primary domains positioned above the stripes, onto which they adsorb (periodic with $\lambda$), but also to the creation of the substructure located above the neutral stripes. A well-ordered substructure is formed when the inherent domain scale $R \sim \lambda/2$ is commensurate with the substrate pattern periodicity.

The formation of the substructure with $\lambda/2$-periodicity depends on the overall area of low-energetic interfaces. To optimize this effect, we have used varying amounts of PMMA to control the compatibility of dPS/PVP interface [8(a)]. The resulting film morphologies of the dPS/PVP/PMMA blend with relative polymer mass fractions 1:1:0, 2:2:1 and 1:1:1 (figs. 5(a), (b) and (c), respectively) all showed $R \sim \lambda/2$. The inspection of the AFM images and a FFT analysis (see caption to fig. 5) indicates that the most effective $\lambda/2$-substructure formation occurs for the 2:2:1 blend. For this blend, the nearly bicontinuous film morphology enhances the substructure formation (resulting also in secondary circular structures), which is lost if the PMMA content is higher [8(a)].

To conclude, spin-coating of polymer blend films can result in well-ordered lateral morphologies with half the periodicity of the underlying substrate pattern. This novel situation, present for commonly encountered conditions (strip-patterned substrates, with one stripe type attracting one blend component [4–6]) and enhanced by optimization (reduced interfacial energy), has important implications for the fabrication of technologically important multiphase polymer films. Ramification of this effect is expected for thicker films with active both lateral and surface-directed phase separation [7].

* * *

We thank Prof. M. Szymoński for the access to the AFM/LFM microscope at the Regional Laboratory for Physical and Chemical Analysis of the Jagellonian University. This work was partly supported by the Reserve of the Rector of the Jagellonian University.

REFERENCES

[1] Binder K., *Adv. Polym. Sci.*, **138** (1999) 1; Budkowski A., *Adv. Polym. Sci.*, **148** (1999) 1.
[2] (a) Rockford L. *et al.*, *Phys. Rev. Lett.*, **82** (1999) 2602; (b) Rockford L., Mochrie S. G. J. and Russell T. P., *Macromolecules*, **34** (2001) 1487.
[3] Fasolka M. J. *et al.*, *Phys. Rev. Lett.*, **79** (1997) 3018; Podariu I. and Chakrabarti A., *J. Chem. Phys.*, **113** (2000) 6423.
[4] Böltau M. *et al.*, *Nature (London)*, **391** (1998) 877.
[5] Cyganik P. *et al.*, *Vacuum*, **63** (2001) 307.
[6] Ermi B. D. *et al.*, *Phys. Rev. Lett.*, **81** (1998) 3900; Nisato G., Ermi B. D., Douglas J. F. and Karim A., *Macromolecules*, **32** (1999) 2356.
[7] (a) Kielhorn L. and Muthukumar M., *J. Chem. Phys.*, **111** (1999) 2259; (b) Shou Z. and Chakrabarti A., *Polymer*, **42** (2001) 6141.
[8] (a) Walheim S., Ramstein M. and Steiner U., *Langmuir*, **15** (1999) 4828; (b) Walheim S. *et al.*, *Macromolecules*, **30** (1997) 4995.
[9] Cyganik P., Budkowski A., Raczkowska J. and Postawa Z., *Surf. Sci.*, **507-510** (2002) 700.
[10] Xia Y. and Whitesides G. M., *Angew. Chem. Int. Ed.*, **37** (1998) 551.
[11] Bernasik A. *et al.*, *Macromol. Rapid. Commun.*, **22** (2001) 829.
[12] (a) Lawrence C. J., *Phys. Fluids*, **31** (1988) 2786; (b) Tanaka H., *Phys. Rev. E*, **51** (1995) 1313; (c) Gutmann J. S., Müller-Buschbaum P. and Stamm M., *Faraday Discuss.*, **112** (1999) 285; (d) Raczkowska J. *et al.*, *Macromolecules*, **36** (2003) 2419.
[13] Sprenger M. *et al.*, *Interface Sci.*, **11** (2003) 225.
[14] Quasi–2-dim phase coarsening process is suggested by the recovery of morphologies similar to thicker films (fig. 2(b)) in the annealed thinner films (fig. 3(d)) (except for the secondary structures, as the role of hydrodynamic and diffusive growth is changed [15]).
[15] Wagner A. J. and Yeomans J. M., *Phys. Rev. Lett.*, **80** (1998) 1429.